Numerical Implementation of 2D-4D modulated Hénon Map and Dynamical Indicators for Orbital Stability in a Circular Accelerator

Marta Razza

June 2, 2024

Contents

Introduction

In this short essay, we will present how the Hénon map allows the description of a particular kind of motion in a circular accelerator, the one in the transverse plane known as the *betatronic motion*. A circular accelerator is made by several magnets, each one with a particular purpose, in this case the focus is on a cell with a sextupolar non-linearity given by the sextupole magnet described by the quadratic Hénon map. The latter will be presented in two different cases: 2-dimensional and 4-dimensional. Then a modulation will be introduced in order to give a description of all these cases in which unavoidable external effects come into play modifying the dynamics of the motion. In the end, some dynamical indicators will be introduced and compared with each other, and some relevant results obtained via a numerical implementation will be shown.

Chapter 1

The Hénon Map

The Hénon Map represents one of the most simple non-integrable models, and the aspect we want to highlight is how in physics it can be used to model a FODO cell with the addition of a sextupolar magnet. The latter consists of a non-linear element inside a magnetic lattice responsible of the reduction of the chromaticity and at the same time an instrument to correct sextupolar errors in the magnets given by feed-down effects. The FODO cell instead represents the fundamental structure of an accelerator formed by a sequence of different magnets each with their own purpose and empty sections, and with a good approximation, it is possible to neglect the edge effects due to the finite dimensions of the magnets. Therefore, in this context, it is possible to perform a discretization of the dynamics because the magnetic fields, placed inside the electromagnets outside the vacuum pipe in a particle accelerator, can be considered as constant along the longitudinal coordinates associated with the orbit.

1.1 The 2-dimensional model

Let's start from the following Hamiltonian function:

$$H = \frac{p^2}{2} + \frac{x^2}{2\beta} - \frac{K_2 x^3}{6} \sum_{n=-\infty}^{+\infty} \delta(s - nl) \tag{1.1}$$

where s represents the longitudinal coordinate defined in $[0, s_L]$ and $l = s_L/L$. This function describes the betatronic oscillations inside an accelerator composed by L FODO cells of lenght l with a sextupole. Then β is the mean of the function β_s over the cell and K_2 represents the gradient of an integrated sextupole; their expressions are:

$$\beta = \frac{1}{l} \int_0^l \beta(s) ds \qquad K_2 = \int_0^{l_s} k_2(s) ds \tag{1.2}$$

where l_s is the sextupole length and $\beta(s)$ is a function related to the transverse plane of the beam. So the equations of motion become:

$$\begin{cases} \dot{x} = p \\ \dot{p} = -\frac{x}{\beta^2} + \frac{K_2}{2} x^2 \sum_{n=-\infty}^{+\infty} \delta(s - nl) \end{cases} \tag{1.3}$$

starting from which, integrating, it is possible to derive the Hénon Map.
First of all we have to consider that $x(s)$ is a continuous variable while $p(s)$ shows discontinuities in $s = nl$ then we can denote the right and the left limits of the discontinuity as $x_n^{\pm}$ e $p_n^{\pm}$, then integrating between $nl - \epsilon$ e $nl + \epsilon$ and considering the limit for which $\epsilon \to 0$, we obtain:

$$\begin{cases} p_n^+ - p_n^- = \frac{K_2}{2} x_n^2 \\ x_n^+ = x_n^- = x_n \end{cases} \tag{1.4}$$

the result is that the map that transforms (x_n, p_n^-) in (x_{n+1}, p_{n+1}^-) can be found computing (x_n, p_n^+), and then adding the term related to the discontinuity:

$$\begin{aligned} \begin{pmatrix} x_{n+1} \\ p_{n+1}^- \end{pmatrix} = \begin{pmatrix} \cos\frac{l}{\beta} & \beta \sin\frac{l}{\beta} \\ -\frac{1}{\beta}\sin\frac{l}{\beta} & \cos\frac{l}{\beta} \end{pmatrix} \begin{pmatrix} x_n \\ p_n^+ \end{pmatrix} = \\ = \begin{pmatrix} \sqrt{\beta} & 0 \\ 0 & \frac{1}{\sqrt{\beta}} \end{pmatrix} \mathbf{R}\left(\frac{l}{\beta}\right) \begin{pmatrix} \frac{1}{\sqrt{\beta}} & 0 \\ 0 & \sqrt{\beta} \end{pmatrix} \begin{pmatrix} x_n \\ p_n^- + \frac{K_2}{2} x_n^2 \end{pmatrix} \end{aligned} \tag{1.5}$$

then introducing a change of coordinates:

$$\hat{x} = \frac{x}{\sqrt{\beta}} \qquad \hat{p} = p\sqrt{\beta} \tag{1.6}$$

and simplifying the notation using a rescaling as follows:

$$\hat{X} = K_2 \frac{\beta^{3/2}}{2} \hat{x} \qquad \hat{P} = K_2 \frac{\beta^{3/2}}{2} \hat{p} \tag{1.7}$$

the two dimensional Hénon map is:

$$\begin{pmatrix} \hat{X}_{n+1} \\ \hat{P}_{n+1} \end{pmatrix} = \mathbf{R}\left(\frac{l}{\beta}\right) \begin{pmatrix} \hat{X}_n \\ \hat{P}_n + \hat{X}^2{}_n \end{pmatrix} \tag{1.8}$$

where $\mathbf{R}(l/\beta)$ can be identified as a rotational matrix.

1.1.1 Modulated 2-dimensional Hénon Map

Introducing the phase advance:

$$\omega = \int_0^l \frac{ds}{\beta} = \frac{l}{\beta} \tag{1.9}$$

the *tune* can be defined as: $Q = \omega/2\pi$.
In this way the matrix found before $\mathbf{R}(l/\beta)$ can be rewritten as:

$$\mathbf{R}(\omega) = \begin{pmatrix} \cos\omega & \sin\omega \\ -\sin\omega & \cos\omega \end{pmatrix} \tag{1.10}$$

and starting from ω, it is possible to introduce a brand new concept: the *tune modulation*. It has a very strong impact on the beam's dynamics, and it causes an increase in long-term particle losses.
The modulation is due to unavoidable external effects such as the coupling between synchrotron and betatron motion (respectively motion on longitudinal and transversal plane) or power supply ripple and can be modelled by a set of non-linear oscillations whose linear frequencies are modulated in the following way:

$$\omega_n = \omega_0 \left(1 + \epsilon \sum_{k=1}^{m} \epsilon_k cos(\Omega_k n) \right) \tag{1.11}$$

Below are shown the parameters ϵ_k e Ω_k related to *Super Proton Synchrotron*:

k	Ω_k	ϵ_k
1	$2\pi/868.12$	$1.000 \cdot 10^{-4}$
2	$2\Omega_1$	$0.218 \cdot 10^{-4}$
3	$3\Omega_1$	$0.708 \cdot 10^{-4}$
4	$6\Omega_1$	$0.254 \cdot 10^{-4}$
5	$7\Omega_1$	$0.100 \cdot 10^{-4}$
6	$10\Omega_1$	$0.078 \cdot 10^{-4}$
7	$12\Omega_1$	$0.218 \cdot 10^{-4}$

Table 1.1: 2-dimensional modulated Hénon Map Parameters

1.1.2 2-dimensional Hénon Map: Numerical Results

In order to better understand what are the main features of Hénon map it was performed a short simulation thanks to which it was possible to extract the phase space portraits below:

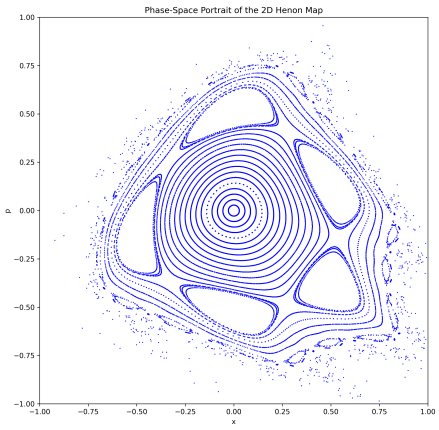

Figure 1.1: Phase-space portrait for Q = 0.210

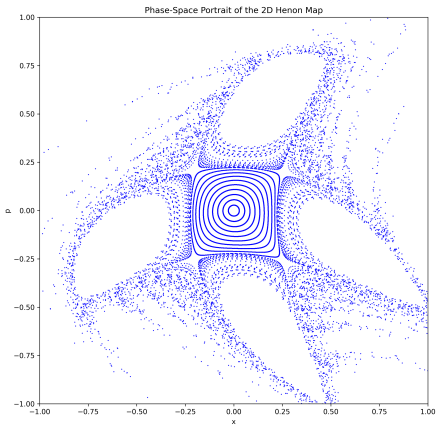

Figure 1.2: Phase-space portrait for Q = 0.254

Looking at the portraits, it is possible to notice that close to the origin orbits are circular while, at a certain point, they become distorted until they become islands. At even larger amplitudes notice the rising of other closed orbits and then the formation of smaller islands. If you have an initial condition inside one island, this will jump from one island to another and then back to the original one; it means that, for instance, in the picture on the left, the five islands are part of the same orbit. If, instead, you are on another closed curve, you simply move along it. The same happens for smaller islands. Another key point to consider is that, beyond a certain amplitude, there are no orbits. This can be understood as a consequence of the quadratic term; in fact, if x is very large, the polynomial term dominates and becomes very large up to infinity. This explains why the non-linear term introduces a sort of limiting amplitude beyond which the particle will reach very large amplitudes so that the particle can go beyond the beam pipe. For the portrait on the right of the figure, the difference is the value of the tune, but it shows the same main features.

1.2 The 4-dimensional model

Considering now the 4-dimensional coordinates written as:

$$\mathbf{x} = \begin{pmatrix} x' \\ p'_x \\ y' \\ p'_y \end{pmatrix} \tag{1.12}$$

and generalizing what we have obtained in the previous section, we can write the 4-dimensional Hénon map as follows:

$$\begin{pmatrix} x' \\ p'_x \\ y' \\ p'_y \end{pmatrix} = \mathbf{L} \begin{pmatrix} x \\ p_x + \frac{K_2}{2}(x^2 - y^2) \\ y \\ p_y - K_2 xy \end{pmatrix} \tag{1.13}$$

in which K_2 is a numerical value that represent the sextupolar strength in the system and $\mathbf{L}$ is the linear part of the transfer map of the lattice. The latter can be rewritten with an appropriate re-scaling as:

$$\mathbf{L} = \begin{pmatrix} R(\omega_x) & 0 \\ 0 & R(\omega_y) \end{pmatrix} \tag{1.14}$$

That is, the generalization of the two-dimensional rotational matrix obtained before. In fact, here $\mathbf{L}$ contains two 2-dimensional rotational matrices.

1.2.1 Modulated 4-dimensional Hénon Map

It is also possible to formulate the tune modulation for the 4-dimensional Hénon map:

$$\begin{pmatrix} x^{(n+1)} \\ p_x^{(n+1)} \\ y^{(n+1)} \\ p_y^{(n+1)} \end{pmatrix} = \mathbf{R} \begin{pmatrix} x^{(n)} \\ p_x^{(n)} + ([x^{(n)}]^2 - [y^{(n)}]^2) \\ y^{(n)} \\ p_y^{(n)} - 2x^{(n)}y^{(n)} \end{pmatrix} \tag{1.15}$$

where:

$$\mathbf{R} = \begin{pmatrix} R(\omega_x^{(n)}) & 0 \\ 0 & R(\omega_y^{(n)}) \end{pmatrix} \tag{1.16}$$

and the linear frequencies are modulated in the following way:

$$\omega_x^{(n)} = \omega_{x0}\left(1 + \epsilon \sum_{k=1}^{m} \epsilon_k \cos(\Omega_k n)\right) \tag{1.17}$$

$$\omega_y^{(n)} = \omega_{y0}\left(1 + \epsilon \sum_{k=1}^{m} \epsilon_k \cos(\Omega_k n)\right) \tag{1.18}$$

where ϵ_k and Ω_k can be varied to obtain the best representation of the characteristics in the real accelerators.

Chapter 2

Analysis of Indicators and Implementation Results

In principle, one is interested into knowing the fate of a particle with given initial conditions in the phase-space after a large number of turns. This is a major problem to assess to design properly the beam pipe, in fact oscillations and non-linearities in the transverse plane can lead to a growth in the space coordinates that overcome the width of the pipe. One may think to follow the particle through its journey up to a very large number of turns, for each possible initial condition. This is a rather long process, for this reason dynamical indicators, borrowed from celestial mechanics, have been implemented to provide an efficient way to study orbital stability.

2.1 Stability Time

Let's now introduce the *stability time* which is based on the fact that, given an initial condition, when the number of iterations is $n = n_{max}$, if its distance from the origin is smaller than a control parameter r_c, we can consider it as *stable*. If, instead, the condition is not satisfied we can consider the initial condition as lost and its tracking is stopped. In this latter case the stability time is given by the first value n_{stab} for which the condition below is valid:

$$\sqrt{x_{nstab}^2 + p_{x,nstab}^2 + y_{nstab}^2 + p_{y,nstab}^2} \geq r_c$$

for the simulation it was used $r_c = 10^2$, but the dependence of the results on the chosen value for r_c is so small that it can be neglected. As previously said, this is an inefficient way to study the orbital stability, for this reason it will be used to compare it with alternative methods.

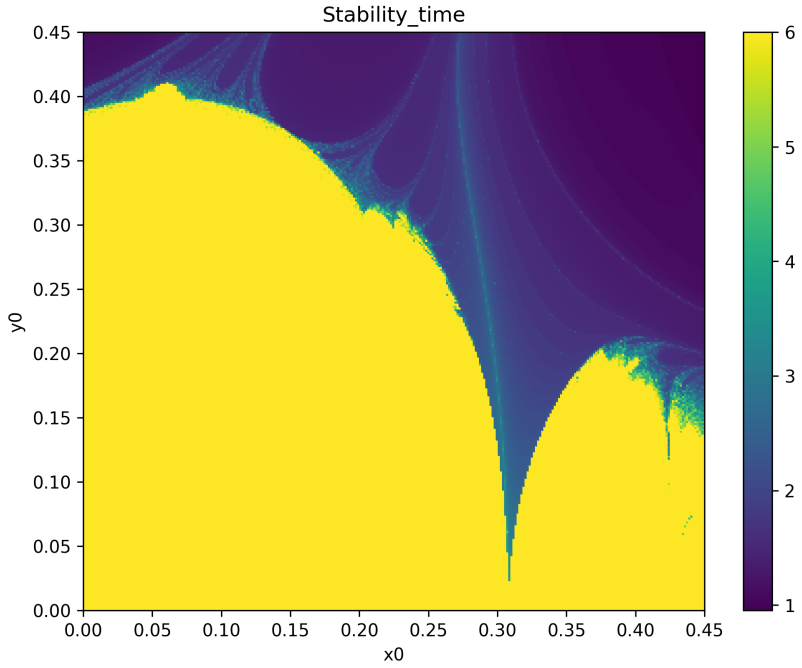

Figure 2.1: Stability time for $Q_x = 0.28$, $Q_y = 0.31$. The tune modulation parameter is $\epsilon = 0$ Initial conditions are evolved up to 10^6. Case: 4D Hénon Map. The number of Stable Samples is: 56044.

2.2 Lyapunov Error

Starting from two initial points $\mathbf{x_0}$ and $\mathbf{y_0} = \mathbf{x_0} + \epsilon\boldsymbol{\eta_0}$, in which $\boldsymbol{\eta_0}$ is a unit vector, and given a symplectic map $\mathbf{M}(\mathbf{x})$ where $\mathbf{x} \in \mathbb{R}^{2d}$, we can write the corresponding orbits $\mathbf{x_n} = \mathbf{M}^n(\mathbf{x_0})$ and $\mathbf{y_n} = \mathbf{M}^n(\mathbf{y_0})$. Let's now consider the n-th normalized displacement:

$$\boldsymbol{\eta}_n = \lim_{\epsilon \to 0} \frac{\mathbf{y_n} - \mathbf{x_n}}{\epsilon} = \lim_{\epsilon \to 0} \frac{\mathbf{M}(\mathbf{y_{n-1}}) - \mathbf{M}(\mathbf{x_{n-1}})}{\epsilon} \tag{2.1}$$

and in analogy with the *directional derivative* for a scalar function$f(x)$:

$$D_v f(\mathbf{x}) = \lim_{h \to 0} \frac{f(\mathbf{x} + h\mathbf{v}) - f(\mathbf{x})}{h} \tag{2.2}$$

which represents the variation of f along $\mathbf{v}$, then for a differentiable f with respect to $\mathbf{x}$ can be written as:

$$D_v f(\mathbf{x}) = \nabla f(x) \cdot \mathbf{v} \tag{2.3}$$

it is possible to derive the following linear recurrence:

$$\boldsymbol{\eta}_n = DM(\mathbf{x}_{n-1})\boldsymbol{\eta}_{n-1} \tag{2.4}$$

from the latter we get to the definition of the *Lyapunov error*:

$$e_n(\boldsymbol{\eta}_0) = \|\boldsymbol{\eta}_n\| = \|DM^n(\mathbf{x_0})\boldsymbol{\eta_0}\| \tag{2.5}$$

Some relations are now reported below in order to get a definition independent of the choice of the initial vector:

$$e_n^L = (Tr(A_n^T A_n))^{1/2} \qquad A_n = DM^n(\mathbf{x}_0) = DM(\mathbf{x}_{n-1})A_{n-1} \tag{2.6}$$

where $A_0 = I$.
Therefore it can be shown that given an orthonormal basis η_{0k}, we have:

$$e_n^L = \left(\sum_{k=1}^{2d} e_n^2(\boldsymbol{\eta}_{0k})\right)^{1/2} \tag{2.7}$$

that represents the expression used in the computational implementation of the Lyapunov error for all the points of the properly spaced lattice in the phase space.

2.2.1 Implementation results for Lyapunov error with a 2-dimensional Hénon Map

Below we can appreciate and understand the importance in using Lyapunov error:

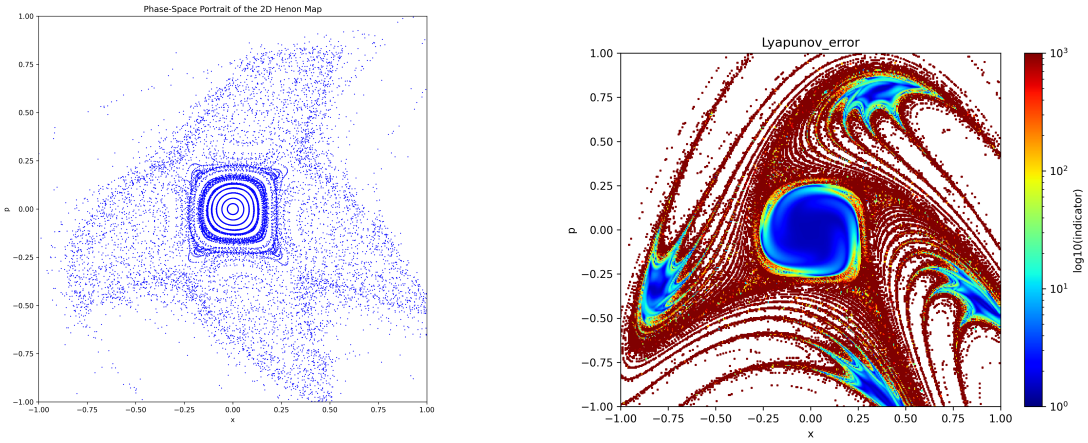

Figure 2.2: Comparison between phase-space portrait and Lyapunov error for $Q_x = 0.254$ and $\epsilon = 64$. Case: 2D Hénon Map

The figure on the left shows clearly the presence of a modulation (the case shown is ϵ =64) but it does not allow to distinguish between stability and instability regions. Instead thanks to the figure on the right we are able to observe directly all the different kinds of region in the phase space.

2.3 Reversibility Error Method

The reversibility error method consists in a procedure in which a given map M is iterated n times and then the correspondent inverse map is in turn iterated n times.
From the deterministic point of view the system should go back to the starting point but computationally it is not the same due to the finite precision of the calculator. It can be shown, in fact, that a numerical breaking of the temporal reversibility is a sufficient condition to determine whether an orbit, in the phase space, is chaotic or not.
An orbit can be classified on the basis of the growth rate of the global error due to the accumulation of *round-off errors* at each map iteration. To understand the behaviour of the global error a plot of the indicator, defined in formula , can be extracted varying the number of iterations. When the orbit is regular the growth of the error will follow a n^{α}-like behaviour, while in case of a chaotic orbit we have an exponential growth as $e^{\lambda n}$, with α, $\lambda \in \mathbb{R}$.
The result of the map and its inverse iterations is compared with the initial condition $\mathbf{x}_0$ through the computation of the norm in order to find the distance between them. This operation allows to get the round-off error. The latter is then divided by the *round-off amplitude* ϵ_r that gives the REM indicator.
Formally:

$$e_n^{REM} = \frac{||M_{\epsilon_r}^{-n} \circ M_{\epsilon_r}^{n}(\mathbf{x_0}) - \mathbf{x}_0||}{\epsilon_r} \tag{2.8}$$

where it was taken $\epsilon_r = 10^{-16}$ for a 8 *byte* representation.

2.3.1 Analysis of stability with REM and Lyapunov Error for a 4D Hénon Map

The definition of a chaotic orbit is evaluated by the distance between the evolution of two nearby initial conditions, this is obtained using *Lyapunov error* that represents ground-truth of chaoticity. It is also possible to use another kind of dynamical indicator like the above mentioned *reversibility error method* which is based on a much simpler implementation since it only requires the direct and inverse evolution of the map. In terms of computational cost the evaluation of tangent map, used in the Lyapunov error, takes instead much more time. Below are shown two colorplots extracted from simulation in which 10^4 iterations are made:

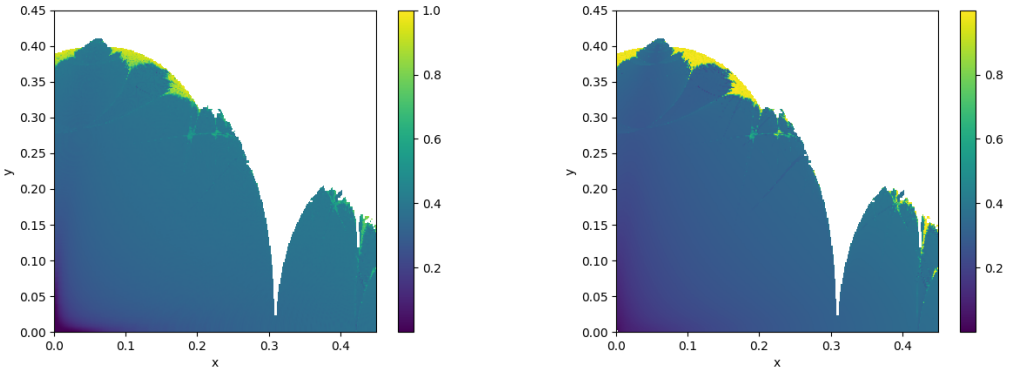

Figure 2.3: Normalized colorplots: on the left for LE and on the right for REM. Number of iterations $= 10^4$, $Q_x = 0.28$ and $Q_y = 0.31$. Initial conditions are taken on a 300×300 lattice on x and y in the interval $[0, 0.45] \times [0, 0.45]$. Stable samples(LE)=56643, Stable samples(REM)=56668.

Chapter 3

Other simulation results

The stable samples are computed for stability time, Lyapunov error and reversibility error method. The case of stability time is different from the other two cases because the stable samples correspond to the maximum value of the stability time meaning that orbits have not exceeded the threshold radius r_c. For a number of iterations equal to 10^6, I have obtained 56044 stable samples. Indicators instead provide the number of stable samples eliminating the values equal to nan or $\pm\infty$ due to numerical saturation.

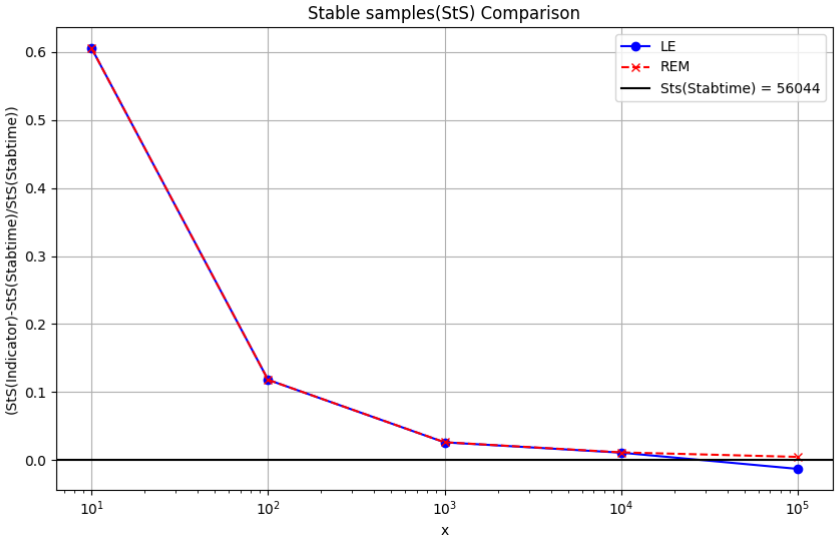

Figure 3.1: Varying the number of iterations shown in the x-axis, the number of stable samples obtained for LE and REM are shown. Already at 10^4 iterations there is a good agreement with the stability time case at 10^6. The number of stable samples was normalized to the one obtained with the stability time.

Another comparison was made in terms of time-performance, below the results:

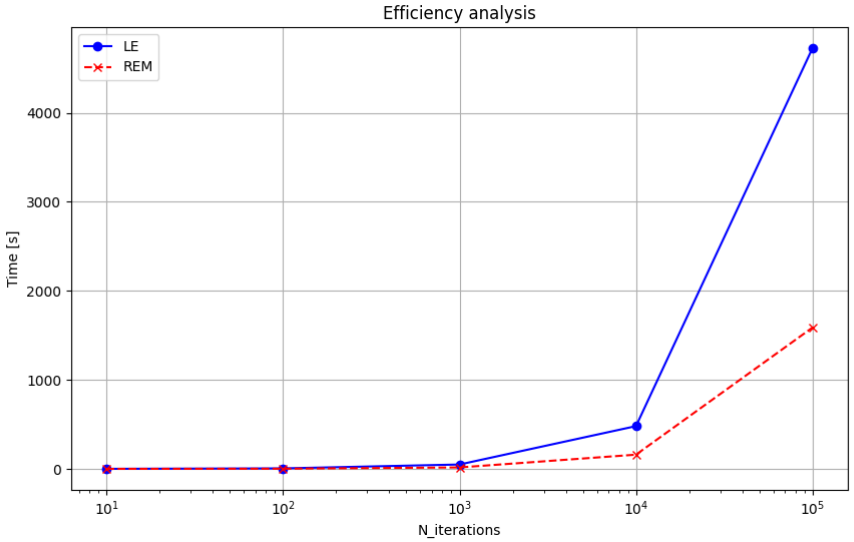

Figure 3.2: The time performance is plotted as a function of the number of iterations. Blue line for LE and red line for REM.

Conclusion

The simulation performed to compute stability time with 10^6 iterations lasts 1 hour and 23 minutes (with my machine) and the result is a number of stable samples = 56044. With the two dynamical indicators it is possible to extract the same results already with 10^4 number of iterations and the duration is extremely lower. Stable samples(LE) = 56643 and Stable samples(REM) = 56668. Furthermore also between the Lyapunov Error and Reversibility error Method there is a difference in terms of time-performance especially when the number of iterations increases.
This analysis is very important because shows that the definition of chaoticity given by the REM and the one given by LE can be considered equivalent. As better explained in the article [2] the Lyapunov error is generally taken as a ground truth for the definition of chaoticity since it considers the different evolution of two nearby initial conditions, but the implementation of REM is much simpler and efficient since it does not require the evolution of the tangent vector in the 4-dimensional hyper-space. Indeed REM requires only the forward and the backward evolution of the Hénon Map.

Bibliography

[1] M.Hénon, C.Heiles, *The Applicability of the Third Integral of Motion: Some Numerical Experiments*, 1964

[2] A. Bazzani, M. Giovannozzi, C.E. Montanari, G. Turchetti, *Performance analysis of indicators of chaos for nonlinear dynamical systems*, 2023

[3] C.E Montanari, *Diffusive models and chaos indicators for non-linear betatron motion in circular hadron accelerators*, 2023

[4] C.E. Montanari, A.Bazzani, M.Giovannozzi, G.Turchetti, *Using Dynamic Indicators for Probing Single-Particle Stability in Circular Accelerators*, 2022

[5] M.Giovannozzi, *Alcuni aspetti di dinamica non lineare con applicazioni in dinamica dei fasci*, 1993

[6] G.Turchetti, F.Panichi, *Fast Indicators for Orbital Stability:A Survey on Lyapunov and Reversibility Errors*, 2019

[7] G.Turchetti, F.Panichi, *Birkhoff normal forms and stability indicators for betatronic motion*, 2019

[8] A.Bazzani, E.Todesco, G.Turchetti, G.Servizi, *A normal form approach to the theory of nonlinear betatronic motion*, 1994

[9] S.Y.Lee, *Accelerator Physics*, Fourth Edition, 2018